Catalysis Science & Technology

PAPER

View Article Online
View Journal | View Issue

Cite this: *Catal. Sci. Technol.*, 2015, 5, 455

Influence of single- and double-flame spray pyrolysis on the structure of MnO_x/γ-Al_2O_3 and FeO_x/γ-Al_2O_3 catalysts and their behaviour in CO removal under lean exhaust gas conditions

Marina Tepluchin,[a] David K. Pham,[b] Maria Casapu,[a] Lutz Mädler,[b] Sven Kureti[c] and Jan-Dierk Grunwaldt*[a]

Received 3rd June 2014,
Accepted 24th August 2014

DOI: 10.1039/c4cy00727a

www.rsc.org/catalysis

MnO_x/Al_2O_3 and FeO_x/Al_2O_3 samples were prepared by two-nozzle flame spray pyrolysis to minimize the formation of composite phases. For this purpose, manganese(II) naphthenate or iron(II) naphthenate and aluminium-*sec*-butylate were sprayed in separate flames and both the structure and the catalytic performance of the materials in CO oxidation were compared to the corresponding single-nozzle flame spray pyrolysis catalysts. Characterization by X-ray diffraction, diffuse reflectance UV-vis spectroscopy and X-ray absorption near-edge structure unravelled that the phases formed in double-flame spray pyrolysis (DFSP) were significantly different from those in single-flame spray pyrolysis; highly dispersed separate entities of manganese/iron oxide and alumina were identified in this case. Despite a slightly lower BET surface area the DFSP prepared samples performed generally better in catalytic CO oxidation than those derived from one single flame. In addition, the manganese-based catalysts were more effective for CO conversion than the corresponding iron-based samples, even at low concentrations.

Introduction

Diesel oxidation catalysis (DOC) is one of the major technologies in exhaust gas aftertreatment systems of lean burn engines to oxidize pollutants, such as CO, non-combusted hydrocarbons and the organic fraction of diesel particulates, to harmless exhaust gas products.[1] For this purpose, usually Pt and Pd catalysts supported on different carriers are used.[2,3] Non-noble metal catalysts such as copper-, nickel- and cobalt-based have also demonstrated significant catalytic activities, for example, in CO oxidation as test reaction.[4,5] Unfortunately, they show lower thermal stability and are sensitive to poisoning.[6,7] Poisoning by sulfur can be easier overcome in future because of ultra-low sulphur contents in gasoline or the use of sulphur-free synthetic fuels.

In addition, unsupported and SBA-15-supported manganese oxide catalysts[8,9] have been tested for this application.[10,11] The following trend for CO oxidation activity was found: $MnO \leq MnO_2 < Mn_2O_3$.[10] Furthermore, the MnO_x-supported catalysts are also promising in NO and soot oxidation.[12,13] In some cases a strong influence of the particle size on the catalytic activity has been found, but this effect is much less pronounced for metal oxide-based catalysts than for noble metal catalysts.[14] In contrast to Mn oxides, only a few studies on Fe-based CO oxidation catalysts were reported.[15,16] Recent DFT calculations showed that Fe_2O_3 nanoparticles particularly with (100) and (0001) surfaces are able to oxidize CO to CO_2 efficiently.[17] Moreover, iron oxide nanoparticles were found to exhibit high catalytic activity for CO, CH_4, and C_3H_6 oxidation.[18]

Different synthesis methods have been used for the preparation of Mn- and Fe-based alumina catalysts such as co-precipitation and conventional incipient wetness impregnation.[19–21] As a function of loading and calcination temperature, various Fe- and especially Mn-based oxide phases can be formed which exhibit different catalytic activities.[8,22,23] In this context, the synthesis by flame spray pyrolysis (FSP) appears to be attractive since it allows the preparation in one step without any additional drying and calcination of the samples and it often leads to high surface area and crystallinity for 10–20 nm length scale nanomaterials.[24–26] This method has already been applied to prepare a number of metal oxide-based particles such as SnO_2, Fe_2O_3, ZrO_2, ZnO and Al_2O_3.[26,27] Furthermore, the method has received strong interest in the exhaust gas

[a] *Institute for Chemical Technology and Polymer Chemistry (ITCP), Karlsruhe Institute of Technology (KIT), Engesserstr. 20, D-76131 Karlsruhe, Germany. E-mail: grunwaldt@kit.edu; Fax: +49 7211 608 44805; Tel: +49 7211 608 42120*
[b] *Department of Production Engineering, Foundation Institute of Material Science (IWT), University of Bremen, Badgasteiner Str. 3, D-28359 Bremen, Germany*
[c] *Institute of Energy Process Engineering and Chemical Engineering (IEC), Technical University of Freiberg, D-09596 Freiberg, Germany*

aftertreatment, *e.g.* for three-way or diesel oxidation catalysts.[28–31] However, incorporation of the catalytically active phase into the alumina carrier or composite formation can be a problem for a standard single-nozzle flame spray pyrolysis system. For example, Strobel *et al.*[32] found the formation of $BaAl_2O_4$ in NO_x-storage-reduction catalysts when spraying barium, aluminium, and Pt precursor solutions together. Høj *et al.*[33] observed the incorporation of Co into the alumina support of Co–Mo/Al_2O_3 catalysts applied for hydrodesulphurization. The group of Choi further reported on the formation of spinel-like $ZnMn_2O_4$ during FSP preparation.[34] In line with these results, binary Fe- and Mn-based γ-alumina CO oxidation catalysts prepared by the FSP method also showed the incorporation of Fe and Mn species, especially for low Mn and Fe loadings (<1 wt.%).[13] Several strategies to avoid the formation of incorporated species during FSP have been reported. Colloidal SiO_2 particles were successfully sprayed for obtaining ZnO–SiO_2 catalysts by Ramin *et al.*[35] An alternative possibility is double-flame spray pyrolysis (DFSP), where the precursor solutions are sprayed in two different flames. This led to the successful formation of, for example, separate alumina and Pt/Ba particles without formation of $BaAl_2O_4$ when DFSP instead of single FSP is used.[32] Using this technique, the formation of $CoAl_2O_4$ could also be prevented when using Co–Mo/Al_2O_3 catalysts, which usually leads to decrease in catalytic activity by hydrodesulphurization,[36] and it was successfully applied for synthesis of alumina-supported cobalt Fischer–Tropsch catalysts.[37]

In the present study, we have systematically investigated the use of double-flame spray pyrolysis for the preparation of Mn/Al_2O_3 and Fe/Al_2O_3 catalysts in comparison to single-flame spray pyrolysis. The materials have been analysed by a number of characterization techniques (BET, XRD, UV-vis, XANES) to unravel whether eventual incorporation of Fe and Mn oxides could be prevented. CO oxidation served as a typical model reaction for environmental catalysts.

Experimental

Preparation of Mn/Al_2O_3 and Fe/Al_2O_3 by flame spray pyrolysis

Setup 1 (University of Bremen). The setup of double-flame spray pyrolysis[36,38] consisted of two separate nozzles, each of them being able to disperse and ignite a liquid precursor solution (Fig. 1). The angle between the two nozzles (φ) was fixed at 120°, the inter-nozzle distance between the angle tip and each nozzle center (d) was 6.2 cm. For the two-nozzle FSP, two separate precursor mixtures were prepared, one containing the Al precursor and the other containing the Mn precursors, or in the case of the Fe/Al_2O_3 catalysts, the Fe precursors. The aluminium precursor solution consisted of aluminium-*sec*-butylate (Alfa Aesar, 97 wt.%) dissolved in xylene (Prolabo, 98.5%). The Al concentration was kept constant at 1 mol l^{-1}. Manganese(II) naphthenate (56 wt.% in mineral spirits, 8% Mn, Alfa Aesar) and iron(II) naphthenate

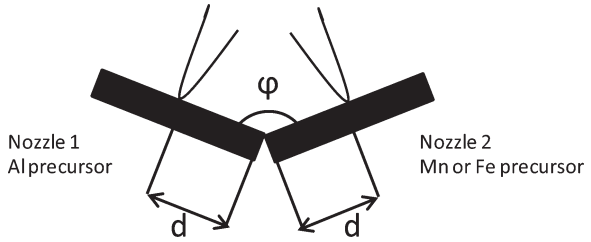

Fig. 1 Sketch of two-nozzle FSP showing the angle between the two nozzles (φ) and the inter-nozzle distance between the angle tip and each nozzle center (d).

(80 wt.% in mineral spirits, 12% Fe, Alfa Aesar) were also dissolved in xylene. The concentrations of manganese and iron were adjusted in a way that the desired Mn and Fe contents in the final catalyst could be obtained. For one-nozzle FSP, the precursor solutions were combined in appropriate amounts into a single solution. For simplification, the samples will be labelled as "X wt.% Fe/Al_2O_3 SF" or "X wt.% Mn/Al_2O_3 DF", demonstrating the content of metal, the type of catalysts and the preparation method, respectively, *e.g.* 2 wt.% Fe/Al_2O_3 DF. In the figures and tables we used "X% Fe SF" and "X% Mn DF".

For two-nozzle FSP, both precursor solutions were fed through capillary tubes at 5 ml min^{-1} using syringe pumps and were dispersed with 5 l min^{-1} high velocity gas flow of oxygen at a 1.5 bar pressure drop from a small annulus around the capillary open end. The spray was ignited with an annular premixed methane flame (3.2 l min^{-1} O_2 and 1.5 l min^{-1} CH_4). The gas flow was controlled by mass flow controllers. The product particles were collected 55 cm above the nozzle onto water-cooled glass-fiber filters (Whatman GF6, 257 mm) in a round filter holder connected to a vacuum pump (Busch SV 1025C). Single-nozzle FSP was performed by spraying the premixed precursor solution of Mn, Fe, and Al at the same setup in one of the flames.

Setup 2 (KIT). Some additional samples were prepared by one-nozzle FSP using the apparatus at KIT. For this purpose, the premixed precursor solution was fed to a capillary tube at 5 ml min^{-1} with a syringe pump and dispersed with 5 l min^{-1} O_2 gas at 4 bar annular nozzle pressure. The spray was ignited by the surrounding premixed CH_4 flame (1.6 l min^{-1} O_2 and 0.76 l min^{-1} CH_4). The powder samples were collected at 40 cm from the nozzle onto a water-cooled glass-fiber filter (Whatman GF6, 240 mm) using a vacuum pump in a round filter holder connected to a vacuum pump (Busch R5). The as-prepared samples are given in Table 1.

Table 1 Prepared samples supported on γ-Al_2O_3

Loading on γ-Al_2O_3 [wt.%]		
Method	Mn	Fe
DF	0.2, 2, 10	0.2, 2, 5, 10, 15, 20, 30
SF	0.2,[a] 2,[a] 10	0.2,[a] 2,[a] 10, 20[a]

[a] Prepared using the setup at KIT.

Catalyst characterization

X-ray diffraction (XRD) patterns were obtained with a Bruker D8 Advance diffractometer using Cu Kα radiation with a Ni filter. XRD scans were recorded with steps of 0.016° in the 2θ range of 20 to 80°. The accelerating voltage and anode current were 40 kV and 35 mA, respectively. Data evaluation was performed using the data bank of the Joint Committee on Powder Diffraction Standards, and the two commercial oxides β-MnO_2 (85%, Merck) and α-Fe_2O_3 (97%, Alfa Aesar) were used for comparison.

X-ray absorption near-edge structure (XANES) experiments were conducted at the XAS beamline at the ANKA synchrotron light source (Karlsruhe, Germany) using a Si (111) double-crystal monochromator detuned to 60 wt.% of the maximum intensity for harmonic rejection. The storage ring was operated at 2.5 GeV and electron currents of 85–180 mA. *Ex situ* measurements were performed using pellets pressed with cellulose. For *in situ* studies (temperature-programmed reaction in 5 vol.% H_2/He), a capillary microreactor heated with a hot air blower (Oxford) was used as described in detail elsewhere.[39,40] Three ionization chambers were used for detecting the incoming and transmitted X-ray intensity of the sample and metallic Mn or Fe foils were measured for energy calibration. For fluorescence detection in the case of 0.2 wt.% samples, an energy-dispersive 5-element solid-state detector (Canberra LeG 5) was used. Normalization of the spectra, energy calibration and background removal were performed with the Athena program of the IFEFFIT package.[41] For comparison, powdered standards of manganese (MnO_2, Mn_2O_3, MnO) and iron (FeO, α-Fe_2O_3, γ-Fe_2O_3, and Fe_3O_4) with known oxidation state and geometry were investigated. Linear combination fitting analysis was performed on the normalized spectra in the −20 to +30 eV range around the absorption energy E_0.

The specific surface areas (SSA) of the as-prepared oxide catalysts were measured by nitrogen adsorption/desorption applying a Belsorp mini II from Bel Japan using multipoint BET in the p/p_0 = 0.05–0.3 range at liquid nitrogen temperature.[42] The error is ±2 to 3 $m^2\ g^{-1}$. Prior to measurements, the samples were degassed at 350 °C in vacuum for 2 h.

Diffuse Reflectance UV-vis spectroscopy data were obtained using a Perkin Elmer spectrometer (Lambda 650) with diffuse reflectance optics. The spectra were collected in the range of 190 to 800 nm with an instrumental resolution of 1 nm. The spectra were analysed using the Kubelka–Munk theory,[43] where $F(R_\infty) = (1 - R_\infty)^2/2R_\infty$. R_∞ is the percentage reflection of an infinite layer of the sample relative to the carrier. The spectra were deconvoluted with Gaussian functions using Origin 8.6.

Catalytic tests

CO oxidation as a catalytic test reaction was conducted in a fixed-bed tubular quartz glass reactor of 8 mm inner diameter at atmospheric pressure in the temperature range of 100–350 °C. The feed consisted of 500 ppm CO, 5 vol.% O_2 and N_2 in balance, with a total flow of 500 ml min^{-1}. 100 mg of the catalyst was diluted with 400 mg of Al_2O_3, loaded in the middle of the quartz glass reactor (as sieved granulate fraction of 125–250 μm) and fixed with two thermocouples in front and behind the catalyst bed to detect the temperature. Before each catalytic test the samples were heated for 30 min in 10 vol.% O_2/N_2 at 350 °C to remove adsorbed water from the surface. CO detection was performed with an online NDIR analyser (Hartmann & Braun, URAS, E10). The CO conversion was calculated based on the inlet and outlet concentrations of CO.

Results and discussion

Characterization

BET surface area. The BET surface areas of samples prepared by DF and SF methods are summarized in Table 2. Mn-based catalysts prepared with DF show a BET surface area of about 90 $m^2\ g^{-1}$ which is almost constant for all loadings. In contrast, the surface area of the corresponding SF samples is slightly higher, reaching 139 $m^2\ g^{-1}$ for the 20 wt.% Mn SF catalyst. This difference may be due to the slightly higher temperature that emerged during double-flame spray pyrolysis including prolonged sintering time of these materials in the flame. The reason for the higher temperature in the two-nozzle flame can be traced back to the fact that the total cold air entrainment of the two-nozzle system is smaller than that in two individual flames.[44] The flame temperature profile is further known to be strongly dependent on the combustion enthalpy of the precursor solution and the flow rate of oxygen dispersion gas, which also influences the surface area.[45] However, these effects seem to be negligible for the Fe-containing catalyst probably due to the more pronounced incorporation phenomena. The BET surface area decreases from 114 to 104 $m^2\ g^{-1}$ for the 10 wt.% Fe/Al_2O_3 SF sample. Nevertheless, due to slightly different parameters of the FSP setup 2 (KIT), *e.g.* the dispersion gas pressure and shorter collection distance,[44,46] the BET surface areas show a small increase with increasing Fe and also Mn loading, *e.g.* 0.2 wt.% Fe shows a BET surface area of 107 $m^2\ g^{-1}$, whereas for 2 wt.% it is 122 $m^2\ g^{-1}$.

X-ray diffraction. The XRD results of the 10 wt.% Mn- and 10 wt.% Fe-containing samples prepared by DF and SF methods are shown in Fig. 2 and unravel γ-Al_2O_3 formation as the only crystalline phase for all catalysts, which has also been previously reported for other alumina-supported FSP catalysts.[32,47] Nevertheless, the formation of δ and θ phases seems to occur under different flame synthesis conditions,

Table 2 BET surface areas of prepared DF and SF samples

Me/γ-Al_2O_3 [wt.%]		0.2	2	5	10	15	20	100
BET [$m^2\ g^{-1}$]	Fe DF	99	93	118	114	117	104	—
	Fe SF	107[a]	122[a]		104			—
	Mn DF	94	95		88			—
	Mn SF	122[a]	131[a]		113		139[a]	—
	Mn_2O_3							43[b]
	Fe_2O_3							19[b]

[a] Prepared at KIT (setup 2). [b] Without Al_2O_3.

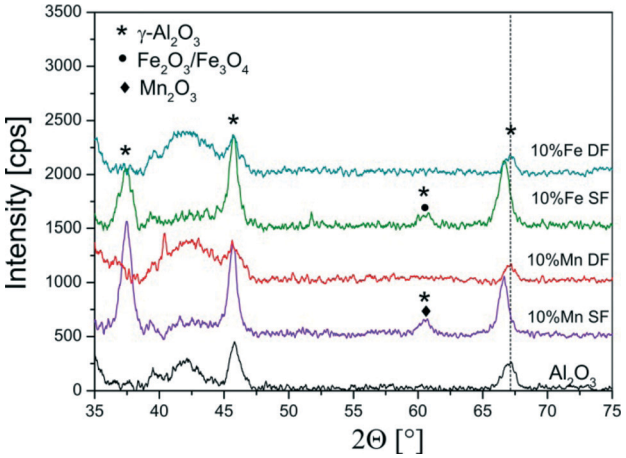

Fig. 2 XRD diffraction patterns of the single- and double-nozzle FSP samples of 10 wt.% Mn- and Fe/Al_2O_3 showing mainly the reflections typical for γ-Al_2O_3 (compare also with ref. 13).

e.g. using $AlCl_3$ as the precursor,[48,49] but the similarly positioned diffraction signals of γ and δ phases make it difficult to distinguish between the two phases unless the particles are large enough, resulting in sharp XRD reflections.[50] No diffraction patterns typical for Mn or Fe oxides have been observed, demonstrating either a homogeneous distribution of the oxides as small particles or the presence of amorphous clusters.[33] Notably, a slight shift in the reflection at $2\Theta = 67°$ was detected, which is shown in Fig. 2 by the dashed line for the SF-prepared samples relative to the γ-Al_2O_3 characteristic XRD pattern. This might indicate the formation of incorporated species or mixed oxides, as observed for similar FSP catalysts[33] and also in line with the reported promoting effect of small ionic radius Mn and Fe cations for γ-Al_2O_3 to α-Al_2O_3 phase transition.[51–53] For a more detailed assessment, the preparation and characterization of Mn–Al or Fe–Al mixed oxide standards followed by Rietveld refinement and using X-rays at a different wavelength source may be useful. In contrast, no shift was observed for the samples prepared by two-nozzle FSP, demonstrating that the MnO_x and FeO_x were not integrated into the γ-Al_2O_3 lattice. Moreover, comparison of diffraction patterns of DF and SF showed the presence of sharper reflections in the case of SF-prepared catalysts, uncovering the formation of more defined crystallites, probably due to the different combustion parameters of the two different setups and/or the higher residence time in the two-flame setup.

Diffuse reflectance UV-vis spectroscopy. The measured DR UV-vis spectra of the as prepared catalysts are shown in Fig. 3 and were deconvoluted using a minimum number of Gaussian curves (*cf.* ref. 54) (for each spectrum, R^2 is about 0.98). A different approach has been conducted by Høj *et al.*,[55] where model compounds for monomeric, dimeric, polymeric and crystalline iron oxide species were measured.

The deconvolution results of the DR UV-vis spectra of 10 wt.% Mn/Al_2O_3 SF show two main absorption bands, one

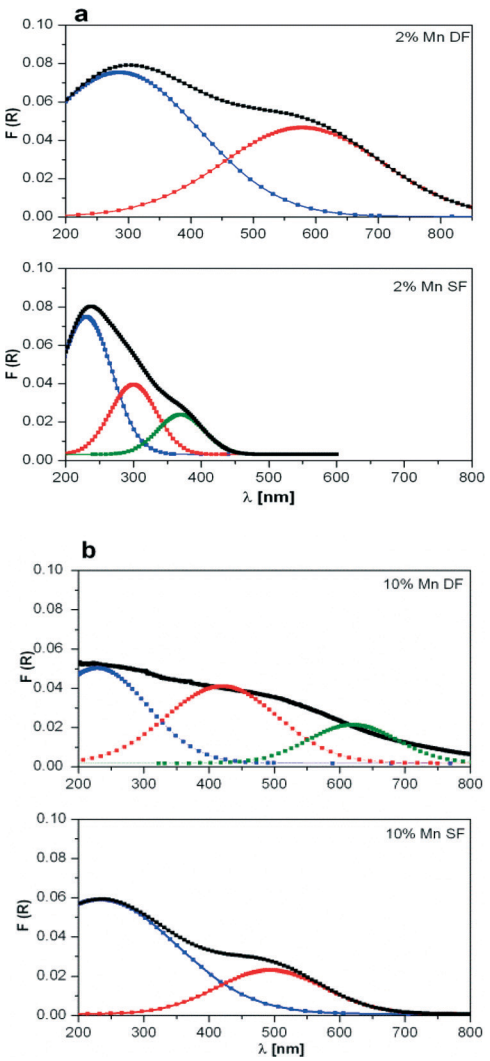

Fig. 3 DR UV-vis spectra of a) 2 wt.% Mn/Al_2O_3 and b) 10 wt.% Mn/Al_2O_3 prepared by DF and SF. For each spectrum, R^2 is about 0.98.

centred near 250 nm and one wide band at about 500 nm which covers almost all of the visible range of the spectrum (Fig. 3b bottom). For the 2 wt.% Mn/Al_2O_3 SF sample only a stronger absorption band at 250 nm with shoulders at 300 and 375 nm was obtained (Fig. 3a bottom). The observed spectra for supported manganese oxides can be interpreted on the basis of literature studies, *e.g.* the study by Stamatis *et al.*[56] According to their results, the first absorption band is associated with an O^{2-} to Mn^{2+} charge transfer transition with Mn located on the surface of alumina, whereas the latter is attributed to badly resolved absorbance bands (d–d transitions) originating from Mn(III) and Mn(IV) oxide species. Possibly, this is also connected to larger clusters of manganese oxides.

Two maxima have been observed for 2 wt.% Mn/Al_2O_3 DF, which shifted toward higher wavelengths in comparison to 2 wt.% Mn/Al_2O_3 SF (Fig. 3a top and bottom, respectively). The absorption spectrum of 10 wt.% Mn/Al_2O_3 DF covers almost the entire visible range up to 800 nm. Three

absorption bands at *ca.* 250, 500 and 650 nm demonstrate the presence of small and larger clusters of $Mn^{2+}/Mn^{3+}/Mn^{4+}$. Particularly, the band at 650 nm evidences the formation of separate metal oxides during the preparation procedure, although they are not visible by XRD.

In the same way, Fe-based catalysts were characterized using DR UV-vis spectroscopy (Fig. 4). A strong overlap of the bands is observed, and again for the elucidation of the different iron species (isolated, polymeric and crystalline iron oxide) up to three Gaussian curves were used for the deconvolution.[54] The spectra, which are depicted in Fig. 4, show an increase in the total absorption area with Fe content in the case of DF-prepared samples, which is in agreement with the literature.[54] The bands are probably due to charge transfer transitions ($O^{2-} \rightarrow Fe^{3+}$).[54,57] The absorption maximum in the region 200–300 nm indicates formation of isolated species (*cf.* assignment of UV-vis bands in ref. 55 and 58). Gaussian curves, which are located in the 300–400 nm range, are assigned to oligomers, and those appearing at higher wavelengths correspond to agglomerated particles, a classification presented earlier by Peréz-Ramírez *et al.*[58] In the case of SF-prepared samples the more pronounced absorption maximum in the 200–300 nm region indicates formation of Fe oxide species incorporated into the alumina and corroborates the XRD results. The broader spectra with contributions at higher wavelengths observed from DF samples suggest the formation of oligomeric species or Fe oxides on the alumina surface. In conclusion, the results indicate that more separate iron and manganese oxide particles or clusters are formed in the case of two-nozzle flame spray pyrolysis which requires further elucidation by other characterization methods.

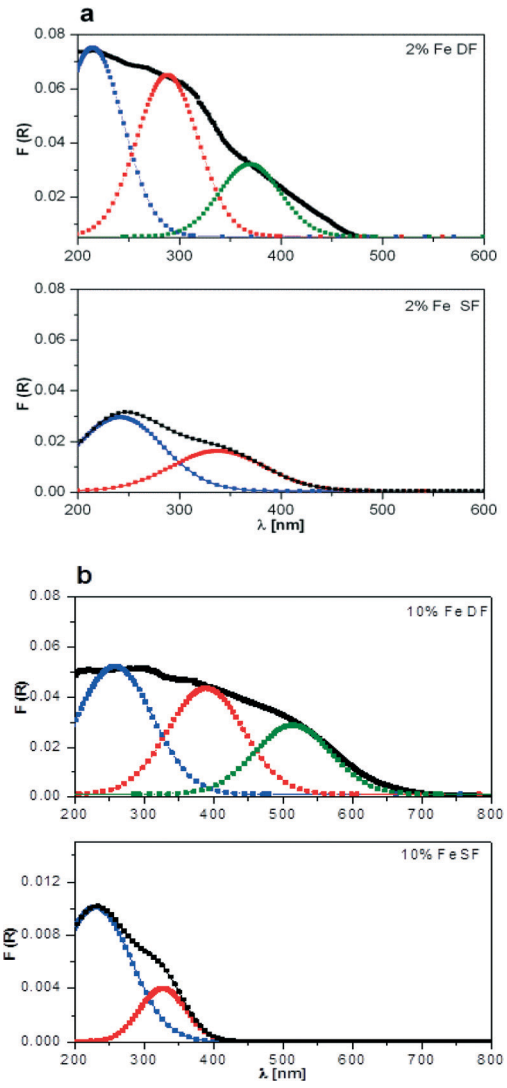

Fig. 4 DR UV-vis spectra of a) 2 wt.% Fe/Al_2O_3 and b) 10 wt.% Fe/Al_2O_3 prepared by DF and SF. For each spectrum, R^2 is about 0.98.

X-ray absorption spectroscopy (XAS). Since the manganese and the iron oxide phases cannot be characterized even for high loadings by X-ray diffraction, the phase composition of selected Mn/Al_2O_3 and Fe/Al_2O_3 samples was further studied by *ex situ* X-ray absorption spectroscopy. The absorption energy and the white line profile of the 3d transition metals are well known to reflect the valence and geometry of the investigated sites.[59] According to a study and theoretical calculations by Farges,[60] the position of the absorption edge can be taken as a direct measure of the oxidation state.[11,59,61] Fig. 5 depicts the XANES spectra collected at the Mn K-edge for DF and SF samples as well as the spectra of Mn oxide references. The profiles and the location of the white line for the 2 and 20 wt.% Mn/Al_2O_3 SF samples as well as for 10 wt.% Mn/Al_2O_3 DF prepared catalyst resemble those of the Mn_3O_4 reference, which correspond to Mn^{3+}/Mn^{2+}cations placed at octahedral and tetrahedral positions. These results are in agreement with the obtained DR UV-vis data and are further elucidated by linear combination fitting (LCF), which gives a more quantitative analysis but strongly depends on the reference spectra used. Mn sites with similar geometry and valence to the reference samples will also result in a similar XANES spectrum.[62–64] According to Table 3 the

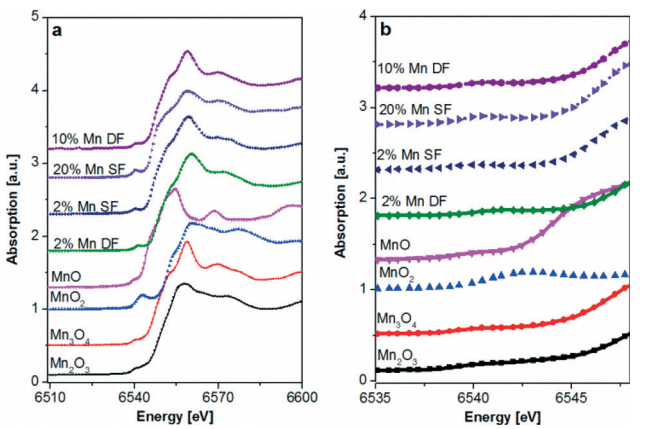

Fig. 5 Mn K-edge XAS spectra of catalysts prepared by DF and SF methods and references, a) XANES region and b) zoom into the pre-edge of the Mn K-edge spectra.

Table 3 Linear combination analysis (LCA) results of as-prepared Mn- and Fe/Al_2O_3 samples obtained from XANES spectra

Reference[a]	2 wt.% Mn DF	2 wt.% Mn SF	10 wt.% Mn DF	20 wt.% Mn SF	Reference[a]	2 wt.% Fe DF	2 wt.% Fe SF	20 wt.% Fe DF	20 wt.% Fe SF
MnO	0.06	0.24	0.03	0.31	FeO	0.10	0	0	0
Mn_2O_3	0.04	0	0	0.15	α-Fe_2O_3	0.10	0	0.30	0
					γ-Fe_2O_3	0.28	0.67	0.23	0.32
Mn_3O_4	0.90	0.76	0.97	0.54	Fe_3O_4	0.52	0.33	0.48	0.68

[a] Reference: Mn and Fe oxides with different oxidation states/geometries used for LCA (*cf.* experimental section).

composition is similar; for the DF samples, a slightly more oxidized overall oxidation state was uncovered by LCF analysis, with more than 90% Mn_3O_4. As it has been previously shown, the formation of different Mn oxides is strongly dependent on temperature. While at about 500 °C and 800 °C amorphous MnO_2 and Mn_2O_3 will form,[65] Mn_3O_4 forms at a calcination temperature above 900 °C.[66] The formation of Mn_3O_4 for all samples as uncovered by XAS might be a result of the high temperature applied during both processes (single- and two-nozzle flame spray pyrolysis[67]).

Moreover, during single-flame pyrolysis the possible formation of mixed Mn–Al oxides with decomposition during cooling in air to highly dispersed defect β-Mn_3O_4 oxide and amorphous Mn–Al–O should also be considered.[50,56] The position of the pre-edge (Fig. 5b) for the 2 and 20 wt.% Mn/Al_2O_3 SF and 10 wt.% Mn/Al_2O_3 DF samples is similar to that of the Mn_3O_4 reference and is further supported by the linear combination analysis results (Table 3).

For both Fe catalysts prepared with double-flame spray pyrolysis an averaged oxidation state of +3 but with an almost equal Fe_2O_3 (α and γ) : Fe_3O_4 phase distribution was obtained from the LCF analysis (Table 3). This is in agreement with DR UV-vis results. Only for the highly loaded 20 wt.% Fe SF sample the white line (especially the pre-edge region in Fig. 6b) is slightly more shifted toward lower energy, uncovering a different coordination environment. The similar structure of iron in γ-Fe_2O_3 and γ-Al_2O_3 together with the observation of isolated species in the case of SF samples in UV-vis supports the idea that the iron is incorporated into the alumina lattice in those cases as also concluded from XRD. In contrast, the 20 wt.% Fe DF sample shows a shift to higher energies evidencing more γ- or α-Fe_2O. (see Fig. 6). This is corroborated by the fitting results in Table 3.

To elucidate the impact of the preparation procedure on the reducibility of the Mn sites, quick EXAFS spectra were collected during temperature-programmed reduction (TPR) experiments in 5 vol.% H_2/He. An earlier onset of the reduction temperature could be linked to an improved low temperature activity in the case of a Mars van Krevelen mechanism.[68] The results of the linear combination fit analysis of the recorded spectra are shown in Fig. 7 and 8, respectively.

Although the 2 wt.% Mn/Al_2O_3 DF sample contains more oxidized Mn sites, the reduction of both catalysts starts as soon as the temperature increases (>60 °C). A continuous reduction was recorded for the 2 wt.% Mn/Al_2O_3 DF so that at the end of the experiment a mixture of Mn^{2+}/Mn^{3+} is present, while the SF catalyst is almost completely reduced to Mn^{2+}. According to the literature, the reduction process follows the trend MnO_2 → Mn_2O_3 → Mn_3O_4 → MnO,[20,69] but the reduction in this case is continuous probably due to the strong interaction of Mn with the oxide surface. For bulk oxides the reduction would be more discrete.[13]

The $E_{0.4}$ energy shift (the energy at 40% of the white line) recorded during the reduction of 2 wt.% Fe/Al_2O_3 DF- as well as for SF-prepared samples indicates the transition from γ-Fe_2O_3 to FeO,[70] with no apparent intermediate step

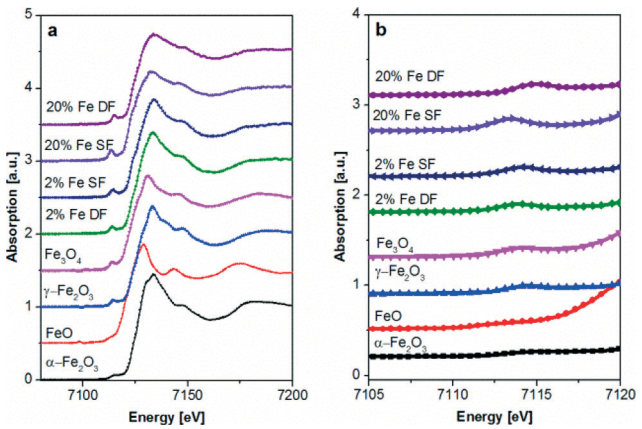

Fig. 6 Fe K-edge XAS spectra of catalysts prepared by DF and SF methods and references. a) XANES region and b) zoom into the pre-edge of the Fe K edge spectra.

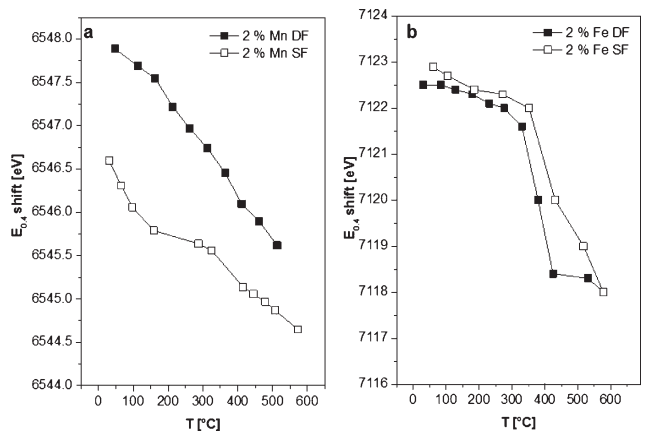

Fig. 7 $E_{0.4}$ shift from samples prepared by DF and SF methods during *in situ* H_2-TPR. a) 2 wt.% Mn/Al_2O_3 DF, 2 wt.% Mn/Al_2O_3 SF and b) 2 wt.% Fe/Al_2O_3 DF, 2 wt.% Fe/Al_2O_3 SF catalysts.

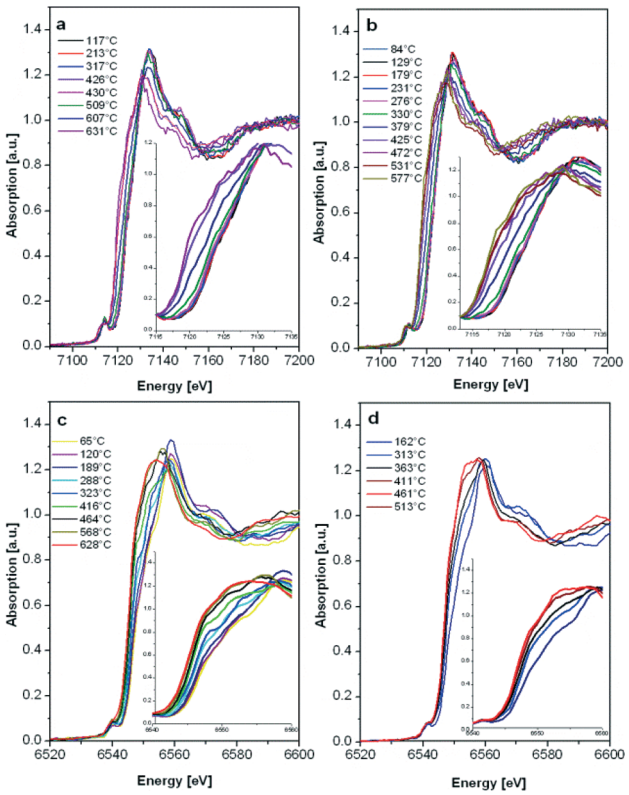

Fig. 8 *In situ* H_2-TPR XANES spectra at the Fe K-edge and the Mn K-edge of 2 wt.% a) Fe/Al_2O_3 SF, b) Fe/Al_2O_3 DF, c) Mn/Al_2O_3 SF and d) Mn/Al_2O_3 DF prepared catalysts. Insets: enlarged white-line region.

(*e.g.* Fe_3O_4 formation). Only a small increase in the reduction onset temperature was observed for the 2 wt.% Fe/Al_2O_3 SF catalyst. In addition, the reduction occurs over a broader temperature regime probably due to a higher dispersion of the Fe sites as shown by DR UV-vis measurements (Fig. 3) or the possible formation of alumina-incorporated species as also evidenced by other characterization methods.

Catalytic performance during CO oxidation

The results of the catalytic activity of SF- and DF-prepared Mn/Al_2O_3 samples are depicted in Fig. 9. The CO conversion increases simultaneously with the Mn content as well as temperature, *i.e.* at 300 °C the CO conversion reaches a maximum of 55% for the 10 wt.% Mn/Al_2O_3 DF sample. Regardless of the different structure evidenced by XRD, DR UV-vis and XAS, the observed data show only little differences in catalytic activity between the catalysts prepared by the two different methods. This is supported by the reducibility of the Mn sites observed between 50 and 300 °C for both 2 wt.% Mn/Al_2O_3 SF and DF catalysts. However, as can be seen for all loadings, the DF samples show slightly higher activity despite the higher surface area of the SF-prepared catalysts.

The catalytic results of DF-prepared Fe/Al_2O_3 samples are shown in Fig. 10 and demonstrate an increase in performance as a function of temperature and Fe loading up to 15 wt.%. For Fe loadings above 20 wt.% the catalytic activity

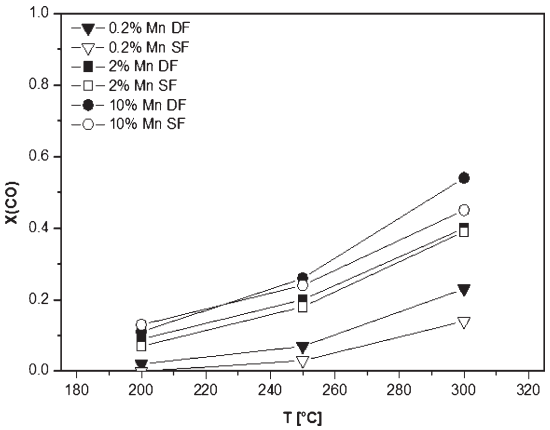

Fig. 9 CO conversions of 0.2, 2 and 10 wt.% Mn/Al_2O_3 catalysts prepared by different methods. Conditions: 100 mg of the catalyst, 500 ppm CO, 5 vol% O_2, balance N_2, total flow 500 ml min^{-1}, GHSV 30 000 h^{-1}.

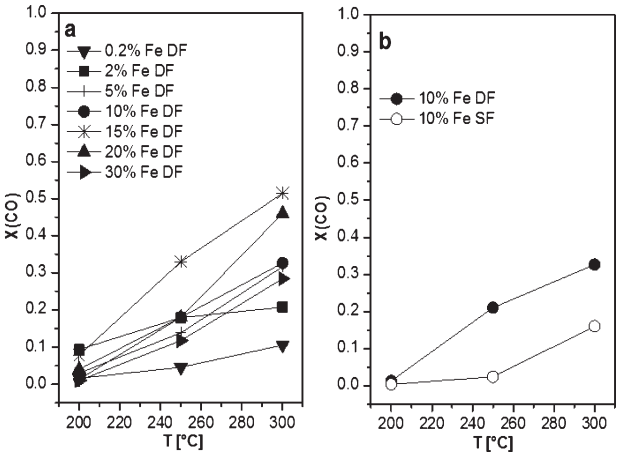

Fig. 10 CO conversions as a function of temperature of a) 0.2, 2, 5, 10, 15, 20 and 30 wt.% Fe/Al_2O_3 prepared by DF and b) 10 wt.% Fe/Al_2O_3 samples prepared by DF and SF. Conditions: 100 mg catalyst, 500 ppm CO, 5 vol.% O_2, balance N_2, total flow 500 ml min^{-1}, GHSV 30 000 h^{-1}.

decreases, which could be caused by the decrease in surface area (Table 1). Compared to the corresponding Mn-based catalyst, the catalytic activity of the 10 wt.% Fe/Al_2O_3 DF sample reaches a maximum of only 34% at 300 °C and of 10% at 200 °C. This is in line with the very limited reducibility of the Fe species as shown by *in situ* XAS-TPR measurements. Nevertheless, the 10 wt.% Fe/Al_2O_3 sample prepared by DFSP exhibited significantly higher CO oxidation activity than the corresponding SF catalyst (10% CO conversion at 300 °C), which is also the case for lower loaded samples (not shown). This tendency is in line with the already observed trend for the Mn-based catalyst series (Fig. 10).

Fig. 11 provides an overview of the activity in terms of turnover frequency (TOF) related to the total number of manganese/iron oxide species and normalized with the surface area of the corresponding catalysts. A superior performance

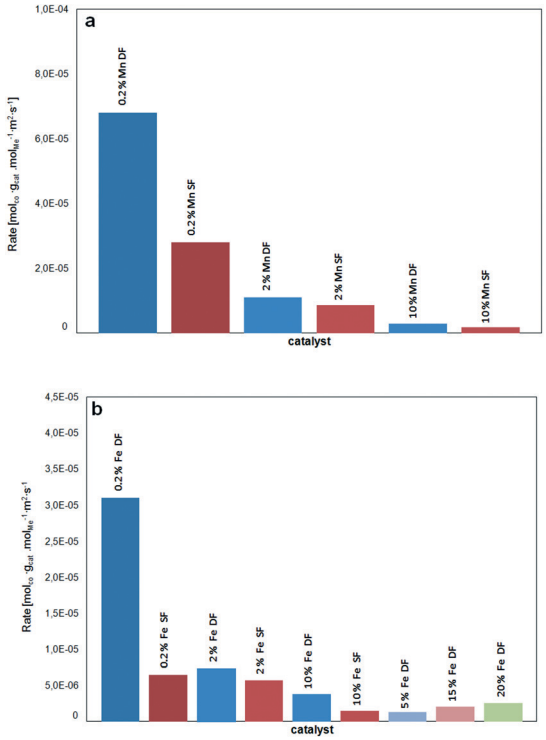

Fig. 11 TOF of a) Mn/Al_2O_3 catalysts and b) Fe/Al_2O_3 catalysts in terms of $mol_{CO}/(mol_{metal}\ s)$ related to the BET surface area ($m^2\ g_{cat}^{-1}$) as a function of catalyst loading and preparation methods.

of the catalysts prepared by DFSP in comparison to the SF samples is especially found in the case of low loaded 0.2 wt.% samples. Hence, this strongly supports the idea that for the DF samples the incorporation of the catalytically active Mn and Fe-species into the alumina support is prevented.

However, in the case of Mn-based catalysts, the composite formation has a much lower influence on the catalytic performance. Apart from their intrinsic higher CO oxidation activity, this could be traced back to the observations of Bulavchenko *et al.*[67] who demonstrated improved CO oxidation activity of the β-Mn_3O_4 phase formed from less active Mn aluminate by phase transformation in O_2, a transformation that is not known for iron–aluminium mixed oxides.

Conclusions

Double-flame spray pyrolysis has been shown to be a suitable method to prevent the formation of incorporated manganese and particularly iron species into the Al_2O_3 lattice which are probably formed during single-flame spray pyrolysis synthesis. Despite a slightly lower surface area some improvements of the catalytic performance could be gained especially for low loaded Mn- and Fe-based samples. Also, the 10 wt.% Fe/Al_2O_3 sample prepared by DF showed a notable increase in the CO oxidation activity. In contrast, only minor differences for manganese-based catalysts with higher loadings (>10%) prepared by DF have been observed. In both cases (SF and DF), the manganese and iron oxides clusters were highly dispersed on the surface, exhibiting oxidation states between Mn(II)/Mn(III) and Fe(II)/Fe(III), respectively. Only the complementary use of several spectroscopic methods allowed tracing of the oxidic structures, and in future it would be of interest to tune the composite formation and to prove it by varying the angle between the two nozzles and the inter-nozzle distance between the angle tip and each nozzle centre. In addition, the stability of the flame-derived catalysts should be studied and compared to conventionally prepared catalysts to further conclude their potential for exhaust gas aftertreatment catalysis. In this respect, finding less costly, efficient and thermally stable non-noble metal catalysts not only for CO oxidation but also for the HC and diesel particulate matter oxidation and NO_x reduction is of high interest, where flame spray methods show high potential.[30]

Acknowledgements

The authors wish to thank ANKA (Karlsruhe, Germany) for providing beam time, Dr. Stefan Mangold for support during the XAS experiments at ANKA-XAS and Dr. Suman Pokhrel for catalyst preparation. We would also like to acknowledge the German Foundation of Environment (Deutsche Bundesstiftung Umwelt) for financing MT's PhD work and the BMBF within the project "Materials in Action" for the support of the setup of the *in situ* infrastructure at the synchrotron radiation source ANKA.

References

1 A. Russell and W. S. Epling, *Catal. Rev.: Sci. Eng.*, 2011, **53**, 337.
2 N. Lopez and J. K. Nørskov, *J. Am. Chem. Soc.*, 2002, **124**, 11262–11263.
3 A. Manasilp and E. Gulari, *Appl. Catal., B*, 2002, **37**, 17.
4 X. Xie, Y. Li, Z.-Q. Liu, M. Haruta and W. Shen, *Nature*, 2009, **458**, 746.
5 S. Royer and D. Duprez, *ChemCatChem*, 2011, **3**, 24–65.
6 G. J. Barnes, *Adv. Chem. Ser.*, 1975, **143**, 72–84.
7 Y. Yao, *J. Catal.*, 1975, **36**, 226.
8 R. Craciun, B. Nentwick, K. Hadjiivanov and H. Knözinger, *Appl. Catal., A*, 2003, **243**, 67–79.
9 Y.-F. Han, F. Chen, Z. Zhong, K. Ramesh and L. C. E. Widjaja, *J. Phys. Chem. B*, 2006, **110**, 24450–24456.
10 K. Ramesh, L. Chen, F. Chen, Y. Liu, Z. Wang and Y.-F. Han, *Catal. Today*, 2008, **131**, 477–482.
11 K. Frey, V. Iablokov, G. Sáfrán, J. Osán, I. Sajó, R. Szukiewicz, S. Chenakin and N. Kruse, *J. Catal.*, 2012, **287**, 30–36.
12 K. Tikhomirov, O. Kröcher, M. Elsener and A. Wokaun, *Appl. Catal., B*, 2006, **64**, 72–78.

13 M. Tepluchin, M. Casapu, A. Boubnov, H. Lichtenberg, D. Wang, S. Kureti and J.-D. Grunwaldt, *ChemCatChem*, 2014, **6**, 1763–1773.
14 V. Schwartz, D. R. Mullins, W. Yan, B. Chen, S. Dai and S. H. Overbury, *J. Phys. Chem. B*, 2004, **108**, 15782–15790.
15 S. Wagloehner, D. Reichert, D. Leon-Sorzano, P. Balle, B. Geiger and S. Kureti, *J. Catal.*, 2008, **260**, 305–314.
16 H. Randall, R. Doepper and A. Renken, *Ind. Eng. Chem. Res.*, 1997, **36**, 2996–3001.
17 A. K. Kandalam, B. Chatterjee, S. N. Khanna, B. K. Rao, P. Jena and B. V. Reddy, *Surf. Sci.*, 2007, **601**, 4873–4880.
18 S. C. Kwon, M. Fan, T. D. Wheelock and B. Saha, *Sep. Pur. Technol.*, 2007, **58**, 40–48.
19 B. R. Strohmeier and D. M. Hercules, *J. Phys. Chem.*, 1984, **88**, 4922–4929.
20 J. Hu, W. Chu and L. Shi, *J. Nat. Gas Chem.*, 2008, **17**, 159–164.
21 Q. Tang, X. Huang, C. Wu, P. Zhao, Y. Chen and Y. Yang, *J. Mol. Catal. A: Chem.*, 2009, **306**, 48–53.
22 S. Cavallaro, N. Bertuccio, P. Antonucci, N. Giordano and J. C. J. Bart, *J. Catal.*, 1982, **73**, 337–348.
23 W. S. Kijlstra, E. K. Poels, A. Bliek, B. M. Weckhuysen and R. A. Schoonheydt, *J. Phys. Chem. B*, 1997, **101**, 309–316.
24 H. K. Kammler, L. Mädler and S. E. Pratsinis, *Chem. Eng. Technol.*, 2001, **24**, 583.
25 R. Strobel, A. Baiker and S. E. Pratsinis, *Adv. Powder Technol.*, 2006, **17**, 457–480.
26 W. Y. Teoh, R. Amal and L. Mädler, *Nanoscale*, 2010, **2**, 1324–1347.
27 R. Strobel, F. Krumeich, W. J. Stark, S. E. Pratsinis and A. Baiker, *J. Catal.*, 2004, **222**, 307.
28 W. Y. Teoh, R. Amal, L. Mädler and S. E. Pratsinis, *Catal. Today*, 2007, **120**, 203–213.
29 R. Strobel, J.-D. Grunwaldt, A. Camenzind, S. Pratsinis and A. Baiker, *Catal. Lett.*, 2005, **104**, 9–16.
30 B. Weidenhof, M. Reiser, K. Stöwe, W. F. Maier, M. Kim, J. Azurdia, E. Gulari, E. Seker, A. Barks and R. M. Laine, *J. Am. Chem. Soc.*, 2009, **131**, 9207–9219.
31 W. J. Stark, J.-D. Grunwaldt, M. Maciejewski, S. E. Pratsinis and A. Baiker, *Chem. Mater.*, 2005, **17**, 3352–3358.
32 R. Strobel, L. Mädler, M. Piacentini, M. Maciejewski, A. Baiker and S. E. Pratsinis, *Chem. Mater.*, 2006, **18**, 2532–2537.
33 M. Høj, K. Linde, T. K. Hansen, M. Brorson, A. D. Jensen and J.-D. Grunwaldt, *Appl. Catal., A*, 2011, **397**, 201–208.
34 S. H. Choi and Y. C. Kang, *Int. J. Electrochem. Sci.*, 2013, **8**, 6281–6290.
35 M. Ramin, N. van Vegten, J.-D. Grunwaldt and A. Baiker, *J. Mol. Catal. A: Chem.*, 2006, **258**, 165–171.
36 M. Høj, D. Pham, M. Brorson, L. Mädler, A. Jensen and J.-D. Grunwaldt, *Catal. Lett.*, 2013, **143**, 386–394.
37 M. Minnermann, S. Pokhrel, K. Thiel, R. Henkel, J. Birkenstock, T. Laurus, A. Zargham, J.-I. Flege, V. Zielasek, E. Piskorska-Hommel, J. Falta, L. Mädler and M. Bäumer, *J. Phys. Chem. C*, 2010, **115**, 1302–1310.
38 M. Minnermann, H. K. Grossmann, S. Pokhrel, K. Thiel, H. Hagelin-Weaver, M. Bäumer and L. Mädler, *Catal. Today*, 2013, **214**, 90–99.
39 J.-D. Grunwaldt, M. Caravati, S. Hannemann and A. Baiker, *Phys. Chem. Chem. Phys.*, 2004, **6**, 3037–3047.
40 J.-D. Grunwaldt, N. van Vegten and A. Baiker, *Chem. Commun.*, 2007, 4635–4637.
41 B. Ravel and M. Newville, *J. Synchrotron Radiat.*, 2005, **12**, 537–541.
42 S. Brunauer, P. H. Emmett and E. Teller, *J. Am. Chem. Soc.*, 1938, 60.
43 L. Yang and B. Kruse, *J. Opt. Soc. Am. A*, 2004, **21**, 1933–1941.
44 M. C. Heine, L. Mädler, R. Jossen and S. E. Pratsinis, *Combust. Flame*, 2006, **144**, 809–820.
45 A. J. Gröhn, S. E. Pratsinis and K. Wegner, *Chem. Eng. J.*, 2012, **191**, 491–502.
46 L. Mädler, in *KONA*, 2004, vol. 22, pp. 107–120j.
47 R. Strobel, W. J. Stark, L. Mädler, S. E. Pratsinis and A. Baiker, *J. Catal.*, 2003, **213**, 296–304.
48 R. M. Laine, J. C. Marchal, H. P. Sun and X. Q. Pan, *Nat. Mater.*, 2006, **5**, 710–712.
49 T. Hinklin, B. Toury, C. Gervais, F. Babonneau, J. J. Gislason, R. W. Morton and R. M. Laine, *Chem. Mater.*, 2003, **16**, 21–30.
50 R. Schlögl, *Bulk Catalysts and Supports*, Wiley-VCH, Weinheim, 1st edn, 1997, vol. 1.
51 G. C. Bye and G. T. Simpkin, *J. Am. Ceram. Soc.*, 1974, **57**, 367–371.
52 K. Okada, A. Hattori, T. Taniguchi, A. Nukui and R. N. Das, *J. Am. Ceram. Soc.*, 2000, **83**, 928–932.
53 F. Maglia, S. Gennari and V. Buscaglia, *J. Am. Ceram. Soc.*, 2008, **91**, 283–290.
54 P. Balle, B. Geiger and S. Kureti, *Appl. Catal., B*, 2009, **85**, 109–119.
55 M. Høj, M. J. Beier, J.-D. Grunwaldt and S. Dahl, *Appl. Catal., B*, 2009, **93**, 166–176.
56 N. Stamatis, K. Goundani, J. Vakros, K. Bourikas and C. Kordulis, *Appl. Catal., A*, 2007, **325**, 322–327.
57 F. Fan, K. Sun, Z. Feng, H. Xia, B. Han, Y. Lian, P. Ying and C. Li, *Chem. – Eur. J.*, 2009, **15**, 3268–3276.
58 J. Pérez-Ramírez, J. C. Groen, A. Brückner, M. S. Kumar, U. Bentrup, M. N. Debbagh and L. A. Villaescusa, *J. Catal.*, 2005, **232**, 318–334.
59 T. E. Westre, P. Kennepohl, J. G. DeWitt, B. Hedman, K. O. Hodgson and E. I. Solomon, *J. Am. Chem. Soc.*, 1997, **119**, 6297–6314.
60 F. Farges, *Phys. Rev. B: Condens. Matter Mater. Phys.*, 2005, **71**, 155109.
61 P. Glatzel, A. Mirone, S. G. Eeckhout, M. Sikora and G. Giuli, *Phys. Rev. B: Condens. Matter Mater. Phys.*, 2008, **77**, 115133–115137.
62 E. Chalmin, F. Farges and G. E. Brown, *Contrib. Mineral. Petrol.*, 2009, **157**, 111–126.
63 F. Farges, *Phys. Rev. B: Condens. Matter Mater. Phys.*, 2005, **71**, 155109.

64 E. López-Navarrete, A. Caballero, A. R. González-Elipe and M. Ocaña, *J. Eur. Ceram. Soc.*, 2004, **24**, 3057–3062.
65 M. Ferrandon, J. Carnö, S. Järås and E. Björnbom, *Appl. Catal., A*, 1999, **180**, 141–151.
66 M. Ferrandon, J. Carnö, S. Järås and E. Björnbom, *Appl. Catal., A*, 1999, **180**, 153–161.
67 O. A. Bulavchenko, T. N. Afonasenko, P. G. Tsyrul'nikov and S. V. Tsybulya, *Appl. Catal., A*, 2013, **459**, 73–80.
68 K. Ramesh, L. Chen, F. Chen, Y. Liu, Z. Wang and Y.-F. Han, *Catal. Today*, 2008, **131**, 477–482.
69 F. Kapteijn, A. D. Vanlangeveld, J. A. Moulijn, A. Andreini, M. A. Vuurman, A. M. Turek, J. M. Jehng and I. E. Wachs, *J. Catal.*, 1994, **150**, 94–104.
70 N. Shah, S. Pattanaik, F. E. Huggins, D. Panjala and G. P. Huffman, *Fuel Process. Technol.*, 2003, **83**, 163–173.